A Numerical Investigation on Oblique Collisions of a Vortex Ring with a Bump

Heng Ren, Hongshan Guan, Wanjun Liu

Abstract— **The interaction of a vortex ring with a bump in three dimensions is investigated using large eddy simulation (LES). We present the vortex structures and divide the evolution of the vortex structures into three different phases. Firstly, when the vortex ring is far from the bump, the flow near the surface of the bump is affected little. Then with the vortex ring approaching the bump, the vortex ring begins to stretch and a boundary layer is generated on the wall. The grow of vorticity in the boundary layer leads to generation of new vortex structures in the flow. Finally, with the strong vortex-vortex and vortex-wall interactions, the large vortex structures break down into small-scale vortices and complex three-dimensional topological structures appear. We investigate effect of distance between symmetry axes of the ring and bump on the evolution of vortical structures. Compared to the case of $L=0.5R_0$, no generation of secondary vortex ring occurs for $L=R_0$. This is mainly due to the breakdown of induced vortex structures at the far end and weak vorticity induced by the primary vortex ring at the near end.**

Index Terms— **Vortex ring, bump, oblique collision, dynamic characteristics.**

[1] INTRODUCTION

The interaction of vortical structures with solid boundaries is a fundamental fluid dynamic topic which has received considerable attention in recent years. The interest in this subject is partly due to several practical applications, (e.g. impact of helicopter rotor vortices with following rotor blades or with the vehicle airframe, chopping of a pump intake vortex by the turbine blades, and interaction of an aircraft trailing vortex with a following aircraft or with the airstrip during landing and take-off), and partially in order to gain a better insight in the fundamental dynamics of vorticity in such flow situations. As one of the simplest and important forms of vortex motion, vortex rings widely exist in nature. The interaction of vortex rings with solid boundaries is an important problem in fluid dynamics. This subject is also associated with a variety of practical applications, such as vortex rings extinguishing gas and oil well fires [1], cavitated rings used for underwater drilling [2], and modeling the interaction between the downburst and the aircraft [3]. Moreover, the underlying flow phenomena and physical mechanisms are still unclear and are of great interest for detailed studies.

Vortex rings interacting with a flat wall has been extensively studied. These studies [4-9] showed that as the primary vortex ring moves gradually toward the wall, its rate of approach slows and its radius continues to increase; meanwhile, considerable secondary vorticity is generated on the surface. When the Reynolds number, based on the initial diameter and translational speed of the vortex ring, is larger than about 500, the secondary vorticity separates from the surface and interacts with the primary vortex ring resulting in the ring rebounding from the wall. Actually, these studies are mainly limited to relatively low Reynolds numbers, the highest Reynolds number in these studies is about 2840 [9]. The experimental study [9] has revealed that, beyond Re = 3000 for the interaction between a vortex ring and a flat wall, the primary vortex ring will no longer remain stable as it approaches the wall.

Comparing with the numerous studies of vortex rings impacting a wall, the work of the interaction between a vortex ring and a curved surface is scarce. This problem is deserved to be further studied. In this paper, we investigate the effect of curvature on the dynamics of the vortical structures by studying the interaction between a vortex ring and an axisymmetric bump. The oblique collision of a vortex ring with a curved surface has never been addressed in the literature.

[2] NUMERICAL METHOD

To investigate a vortex ring impinging on a curved surface, the three-dimensional Favre-filtered compressible Navier-Stokes equations in generalized coordinates are employed. The equation of state for an ideal gas is used and the molecular viscosity is assumed to obey the Sutherland law. To non-dimensionalize the governing equations, the radius of the initial vortex ring and the far-field variables are used as characteristic quantities. It should be indicated that, similar to LES on the evolution of longitudinal stationary vortices [10], the present simulation is for a low Mach number of 0.3 based on the far-field speed of sound, which is very near the incompressible limit. Sreedhdar and Ragab [10] have verified that the approach based on the compressible N-S equations can reliably predict the incompressible flow characteristics of the vortex evolution.

The large eddy simulation is implemented for turbulence closure. In order to model some terms in the Favre-filtered equations arising from the unresolved scales, dynamic subgrid-scale (SGS) models for turbulent flows are employed. A detailed description of the mathematical

Manuscript received Jan 5, 2015.

Heng Ren, *China Electronics Technology Group Corporation No.38 Research Institute,* (*e-mail: renheng_cetc38@163.com*). *Hefei, China, +86 18900518514.*

Hongshan Guan, *China Electronics Technology Group Corporation No.38 Research Institute, Hefei, China, +86 13855113863.*

Wanjun Liu, *China Electronics Technology Group Corporation No.38 Research Institute, Hefei, China.*

ISSN: 2278 – 7798

formulation of the governing equations and the SGS models have been given in our previous paper [11-12].

The governing equations are numerically solved by a finite-volume method. As employed in our previous work [11-12], the convective terms are discretized by a second-order central scheme and the viscous terms by a fourth-order centered scheme. Time advancement is performed by an implicit approximate factorization method with sub iterations to ensure a second-order accuracy. Moreover, the present numerical methods have already been used successfully to a variety of turbulent flows and have been verified to provide the reliable calculations.

[3] COMPUTATIONAL OVERVIEW AND VALIDATION

As illustrated in Fig. 1, a vortex ring of radius R_0 is initially placed at $\boldsymbol{x}_c = (0, L, h)$, the distance between the ring and the flat wall is $h = 6R_0$. The bump has a circular base, with a cosine-squared cross section and the shape is defined as

$$z(x, y) = H \cos^2\left(\frac{\pi\sqrt{x^2 + y^2}}{6}\right). \quad (1)$$

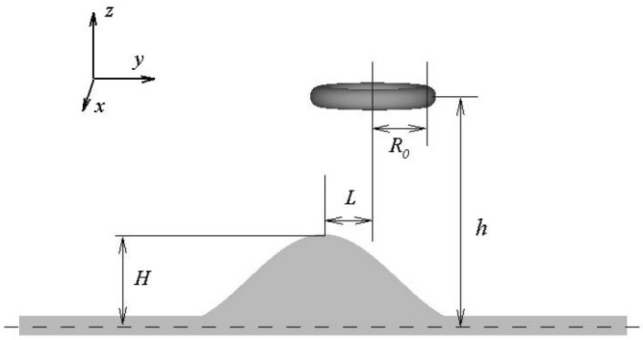

Fig. 1. Schematic diagram of a vortex ring approaching a bump.

The initial vorticity distribution of the vortex ring is assigned by a Gaussian function. The initial translational speed of the vortex ring can be represented as [13]

$$u_v = \frac{\Gamma}{4\pi R_0}\left(\ln\frac{8R_0}{\sigma_0} - \frac{1}{4}\right), \quad (2)$$

where σ_0 is the initial core radius and Γ is the circulation of the vortex ring. To deal with the instability of the vortex ring, an azimuthal disturbance with an amplitude of 2×10^{-4} is introduced by imposing a radial displacement on the axis of the ring [14].

In the computation, we calculate two cases with $L = 0.5R_0$ and R_0. The height of the bump is $H = 1.8R_0$. Slenderness ratio of the vortex ring is $\sigma_0 / R_0 = 0.2$ and the initial translational speed of the ring is $u_s = 0.3$. Reynolds number based on the translational speed and ring diameter is $Re = 4 \times 10^4$, and the corresponding Reynolds number based on circulation of the vortex ring is $\mathrm{Re}_\Gamma = 7.27 \times 10^4$.

The computational domain extends for 16 ring radii in the x and y directions and 12 radii in the vertical direction, with $L_x/R_0 = L_y/R_0 = 16$, $L_z/R_0 = 12$. Based on our careful examinations, a mesh of size $N_x \times N_y \times N_z = 641 \times 641 \times 237$ with resolution $R_0 = 40\Delta x$ is used in the computation, where N_x and N_y are two lateral dimensions of the mesh in two horizontal directions x and y, and N_z is the dimension in the vertical direction z. The grid-spacing is uniform in x and y, and grid stretching is employed in z to increase the grid resolutions near the surface. In the transversal x and y directions, periodicity boundary conditions are used. In the vertical z direction, the flow is bounded by a no-slip wall on the bump surface and far-field boundary condition at $z = L_z$.

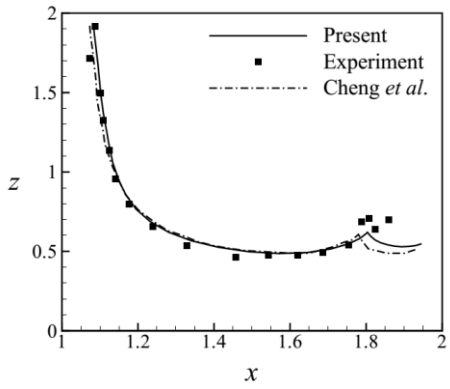

Fig. 2. The trajectory of the primary ring center for $Re = 830$. The solid and dashdot lines present the numerical results obtained in this work and by Cheng *et al*. respectively. The symbol represents the experimental data.

We will validate our code by a comparison with the existing results for a vortex ring impacting a flat wall at $Re = 830$. For the vortex ring/wall interacting case, the initial conditions are the same with experiment by Chu *et al*. [8]. The Gaussian ring is initially placed at the vertical position $h = 3R_0$ and we use the grid resolution $R_0 = 30\Delta x$ for the simulation which is same with the cases in Cheng *et al*. [4]. We compare the trajectory of the primary vortex ring center with the experiment and the numerical study, as shown in Fig. 2. Clearly, our results are convergent to the experimental data and better than numerical results by Cheng *et al*. using Lattice Boltzmann method.

[4] RESULTS AND DISCUSSION

We first discuss the complex flow structures. Fig. 3 shows the evolution of three-dimensional vortex structures depicted by isosurface of the Q-criterion for the two cases. The dynamic process for the case of $L = 0.5R_0$ is similar to the interaction between a vortex ring and a flat plate, as shown in Fig. 3 (a). A sequence of events takes place when a vortex ring approaches a bump. Firstly, when the vortex ring is close to the bump, the ring entrains surrounding fluids and a thin boundary layer is generated on the surface. Secondly, as the ring moves closer to the bump, it begins to stretch and the induced boundary layer grows rapidly. And thirdly, after $t \geq 15.0$, the boundary layer undergoes separation in the adverse pressure gradient region leading to ejection of vorticity generated on the surface into the surrounding fluid. At $t = 20.0$, we observe a second vortex ring is generated. It lifts up from the wall and then interacts with the primary ring. The interaction between the primary and secondary rings decelerates the radial expansion of the primary ring and causes the primary ring to rebound from the wall. Then the primary ring further induces an additional separation of the boundary layer to generate a tertiary vortex ring, which is weak than the secondary vortex ring. At $t = 22.5$, we observe the secondary ring develops a helical structure. This is mainly

ISSN: 2278 – 7798

due to the growth of azimuthal instability, which is sensitive

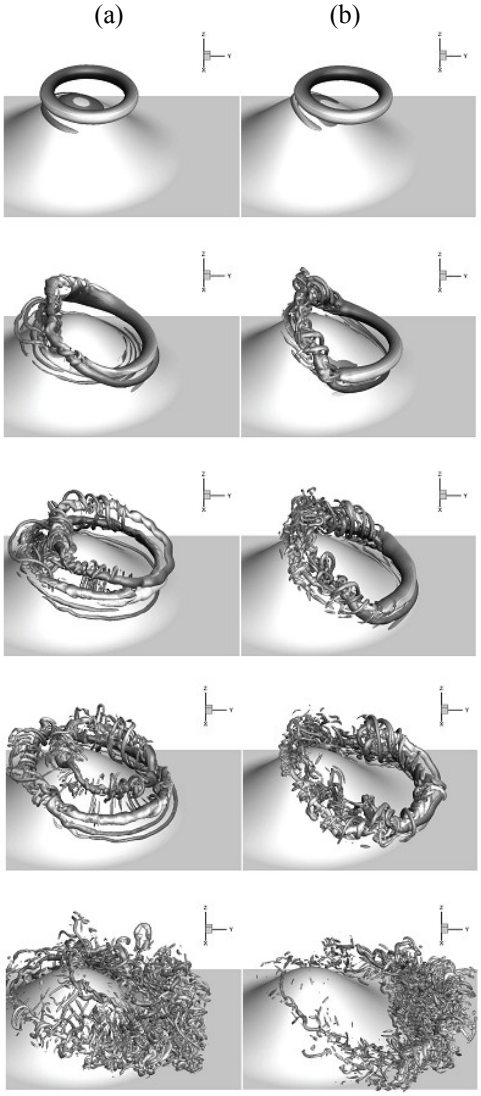

Fig. 3. Evolution of vortex structures shown by isosurface of the Q-criterion ($Q = 3$). (a) $L = 0.5R_0$, (b) $L = R_0$. Evolution is from top to bottom and shown at times t = 15.0, 20.0, 22.5, 25.0, 35.0.

to vortical structures at high Reynolds number. Then the secondary vortex ring is convected inward to the center of the primary ring and begins to interact with the bump. After t = 25.0, the strong vortex-vortex and vortex-wall interactions lead to breakdown of vortex structures into small-scale vortices and complex three-dimensional topological structures appear.

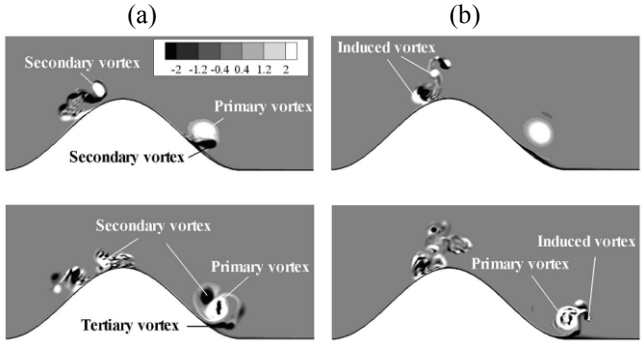

Fig. 4. The x-vorticity ω_x field in the $x = 0$ plane. (a) $L = 0.5R_0$, (b) $L = R_0$. Evolution is from top to bottom and shown at times t = 20.0 and 25.0.

When the distance between the symmetry axes of the ring and bump is increased to $L = R_0$, the evolution of vortex structures is shown in Fig. 3 (b). At t = 22.5, compared to the case of $L = 0.5R_0$, the induced vortex on the surface does not lift up from the wall and no secondary vortex ring is generated for $L = R_0$. This is the main difference between the two cases.

In order to more clearly show the difference between the two cases, we give the vorticity field in the $x = 0$ plane, as shown in Fig. 4. At t = 20.0, we observe the secondary vortex at the near end is separating from the wall for the case of $L = 0.5R_0$. While for $L = R_0$, the vorticity at the near end is weak. Then at t = 25.0, the secondary vortex at the near end has moved inward to the primary vortex. While for the case of $L = R_0$, at this time, the weak induced vorticity has just separated from the wall.

We then discuss the evolution of energy and enstrophy in the whole domain, as shown in Fig. 5. The kinetic energy E and Ω are defined as

$$E = \frac{1}{2}\int (\boldsymbol{u}\cdot\boldsymbol{u})dV, \tag{3}$$

$$\Omega = \frac{1}{2}\int (\boldsymbol{\omega}\cdot\boldsymbol{\omega})dV, \tag{4}$$

For the case of $L = 0.5R_0$, we divide the interaction of the ring with the bump into three distinct phases: approach, slowing and collision. During the approach phase ($0 \le t \le 10$), the vortex ring is far from the bump and the enstrophy is almost constant. The initial fast decrease of kinetic energy is attributed to the reorganization of the flow field, due to the unphysical nature of the initial random perturbations. Once the flow adjust itself, the energy decreases monotonically and slowly mainly due to the viscous dissipation of the flow. During the slowing phase ($10 \le t \le 15$), the kinetic energy begins to decrease rapidly. After t = 15.0, the ring enters the collision phase. The enstrophy firstly grows considerably due to the separation of boundary layer and generation of secondary vortex ring. Then it increases slows down and almost comes to a halt during $20.5 \le t \le 24.0$. After t = 24.0, with the generation of tertiary vortex ring and stretching of the primary and secondary vortex rings, the enstrophy increases again and gets its maximal value at t = 32.5. After t = 32.5, with no generation of new vortex in the flow and breakdown of vortex structures into small-scale vortices, the enstrophy decreases rapidly.

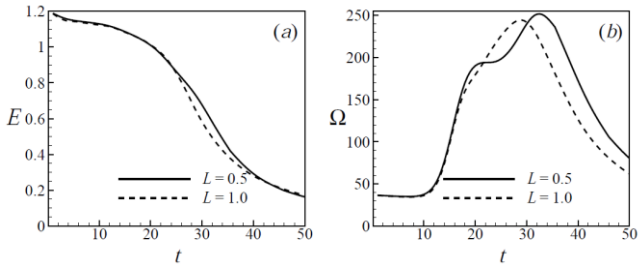

Fig. 5. Evolution of integrated kinetic energy (a) and enstrophy (b) in the whole domain.

For the case of $L = R_0$, from t = 24.0, the energy begins to decrease more rapidly than $L = 0.5R_0$. This is mainly due to the interaction between the induced vortex and the primary vortex ring at the far end. We also observe the enstrophy for $L = R_0$ increases monotonically and no second increase occurs

ISSN: 2278 – 7798

before the enstrophy gets its maxima value. This is mainly due to continuous stretching of primary vortex ring and no generation of secondary vortex ring respectively.

In Fig. 6, we give the instantaneous strain-rate field in the $x = 0$ plane. For the both two cases, after the near end of vortex ring contacts with the bump, the stretching of vortex structures is stronger. This is corresponding to the increase of enstrophy in Fig. 5 (b).

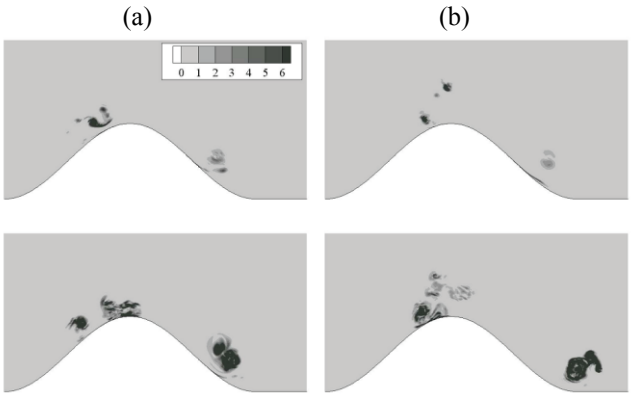

Fig. 6. Distributions of the instantaneous strain-rate magnitude in the x=0 plane. (a) $L = 0.5R_0$, (b) $L = R_0$. Evolution is from top to bottom and shown at times $t = 20.0$ and 25.0.

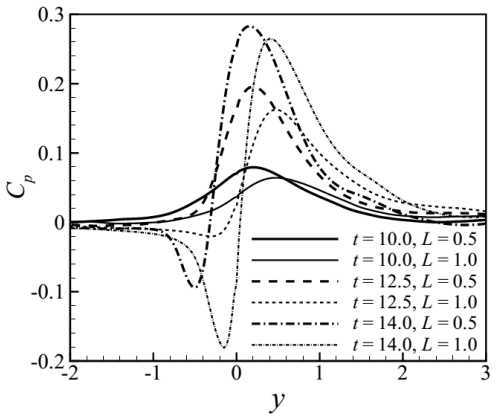

Fig. 7. Pressure coefficient variation along the $x = 0$ line on the surface.

We give the pressure coefficient variation along the $x = 0$ line on the bump surface for the two cases, as shown in Fig. 7. Before $t = 12.5$, as the vortex ring approaches the bump, the positive pressure on the surface increases rapidly. At $t = 14.0$, the negative pressure coefficient appears and mainly distributes beneath the far end of the vortex ring. Then the absolute values of the positive and negative pressure coefficients at the far end decrease rapidly. After the near end of the vortex ring collides with the bump, the minimum negative pressure coefficient occurs on the wall at $y = 2.1$. Eventually, with the breakdown of vortex structures, the impact of the vortex structure on the pressure is weak and the pressure coefficient oscillates around the zero value.

[5] CONCLUSION

The interaction between a vortex ring and a three-dimensional bump has been studied by means of the large eddy simulation technique. The vortical flow phenomena and the underlying physical mechanisms were investigated and are summarized briefly as follows.

As a vortex ring impinges on a bump, an array of vortical flow phenomena occur, such as the generation and deformation of secondary vortex ring, the formation of loop-like vortices, the interaction of vortex rings, and the instability and breakdown of vortical structures. The total kinetic energy and enstrophy have been investigated to reveal the different stages of flow evolution. The main difference between the two cases is no generation of secondary vortex ring occurs for the case of $L = R_0$. This is mainly due to the breakdown of induced vortex structures at the far end and weak vorticity induced by the primary vortex ring at the near end.

REFERENCES

[1] D. G. Akhmetov, B. A. Lugovtsov, and V. F. Tarasov, "Extinguishing gas and oil well fires by means of vortex rings," *Combust. Explos. Shock Waves*, vol. 16, pp. 490-494, 1980.

[2] G. L. Chahine, and P. F. Genoux, "Collapse of a cavitating vortex ring," *J. Fluid Eng.*, vol. 105, pp. 400-405, 1983.

[3] T. S. Lundgren, and N. N. Mansour, "Vortex ring bubbles," *J. Fluid Mech.*, vol. 224, pp. 177-196, 1991.

[4] M. Cheng, J. Lou, and L. S. Luo, "Numerical study of a vortex ring impacting a flat wall," *J. Fluid Mech.*, vol. 660, pp. 430-455, 2010.

[5] T. T. Lim, T. B. Nickels, and M. S. Chong, "A note on the cause of rebound in the head-on collision of a vortex ring with a wall," *Exp. Fluids.*, vol. 12, pp. 41-48, 1991.

[6] P. Orlandi, and R. Verzicco, "Vortex rings impinging on walls: axisymmetric and three dimensional simulations," *J. Fluid Mech.*, vol. 256, pp. 615-646, 1993.

[7] A. M. Naguib, and M. M. Koochesfahani, "On wall-pressure sources associated with the unsteady separation in a vortex-ring/wall interaction," *Phys. Fluids.*, vol. 16, pp. 2613-2622, 2004.

[8] C. C. Chu, C. T.Wang, and C. C. Chang, "A vortex ring impinging on a solid plane surface-Vortex structure and surface force," *Phys. Fluids A*, vol. 7, pp. 1391-1401, 1995.

[9] J. D. A. Walker, C. R. Smith, A. W. Cerra, and T. L. Doligalski, "The impact of a vortex ring on a wall," *J. Fluid Mech.*, vol. 181, pp. 99-140, 1987.

[10] M. Sreedhdar, and S. Ragab, "Large eddy simulation of longitudinal stationary vortices," *Phys. Fluids*, vol. 6, pp. 2501-2514, 1994.

[11] H. Ren, and X.Y. Lu, "Large eddy simulation of a vortex ring impinging on a three-dimensional circular cylinder," *Theor. Appl. Mech. Lett.*, vol. 3, 032007, 2013.

[12] H. Ren, and C. Y. Xu, "Three-dimensional numerical simulation of a vortex ring impacting a bump," *Theor. Appl. Mech. Lett.*, vol. 4, 032004, 2014.

[13] P. G. Saffman, "The number of waves on unstable vortex rings," *J. Fluid Mech.,* vol. 84, pp. 625-639, 1978.

[14] K. Shariff, R. Verzicco, and P. Orlandi, "A numerical study of three-dimensional vortex ring instabilities: viscous corrections and early nonlinear stage," *J. Fluid Mech.,* vol. 279, pp. 351-375, 1994.

Heng Ren received B. E. degree in Engineering Mechanics from Lanzhou University and Ph. D degree in Engineering Mechanics from University of Science and Technology of China. Presently working as an engineer in China Electronics Technology Group Corporation No.38 Research Institute. His research areas are electronic equipment thermal control and computational fluid dynamics.

Hongshan Guan received B. E. degree in Engineering Thermophysics from Nanjing University of Aeronautics and Astronautics. Presently working as a senior engineer in China Electronics Technology Group Corporation No.38 Research Institute. His research areas are radar structure design and electronic equipment thermal control.

Wanjun Liu working as an engineer in China Electronics Technology Group Corporation No.38 Research Institute. His research areas are radar structure design and electronic equipment thermal control.

ISSN: 2278 – 7798